The Astrophysical Journal, 945:87 (9pp), 2023 March 10 https://doi.org/10.3847/1538-4357/acbc7d

A Measurement of Circumgalactic Gas around Nearby Galaxies Using Fast Radio Bursts

Xiaohan Wu[1,2] and Matthew McQuinn[3]
[1] Canadian Institute for Theoretical Astrophysics, University of Toronto, Toronto, ON, M5S 3H8, Canada; xwu@cita.utoronto.ca
[2] Harvard-Smithsonian Center for Astrophysics, 60 Garden Street, Cambridge, MA 02138, USA
[3] Astronomy Department, University of Washington, Seattle, WA 98195, USA
Received 2022 September 13; revised 2023 February 13; accepted 2023 February 14; published 2023 March 9

Abstract

The distribution of gas in the circumgalactic medium (CGM) of galaxies of all types is poorly constrained. Foreground CGMs contribute an extra amount to the dispersion measure (DM) of fast radio bursts (FRBs). We measure this DM excess for the CGMs of 10^{11}–$10^{13}\,M_\odot$ halos using the CHIME/FRB first data release, a halo mass range that is challenging to probe in any other way. Because of the uncertainty in the FRBs' angular coordinates, only for nearby galaxies is the localization sufficient to confidently associate them with intersecting any foreground halo. Thus we stack on galaxies within 80 Mpc, optimizing the stacking scheme to approximately minimize the stack's variance and marginalize over uncertainties in FRB locations. The sample has 20–30 FRBs intersecting halos with masses of 10^{11}–$10^{12}\,M_\odot$ and also of 10^{12}–$10^{13}\,M_\odot$, and these intersections allow a marginal 1σ–2σ detection of the DM excess in both mass bins. The bin of 10^{11}–$10^{12}\,M_\odot$ halos also shows a DM excess at 1–2 virial radii. By comparing data with different models for the CGM gas profile, we find that all models are favored by the data up to 2σ level compared to the null hypothesis of no DM excess. With 3000 more bursts from a future CHIME data release, we project a 4σ detection of the CGM. Distinguishing between viable CGM models by stacking FRBs with CHIME-like localization would require tens of thousands of bursts.

Unified Astronomy Thesaurus concepts: Radio bursts (1339); Radio transient sources (2008); Circumgalactic medium (1879)

1. Introduction

The circumgalactic medium (CGM)—the diffuse gas that sits outside galaxy disks and inside the virial radii of halos—is a crucial component in the baryonic processes in the universe. It receives inflow of the intergalactic gas, fuels star formation in galaxies, and bears the impact of galactic feedback (Naab & Ostriker 2017; Tumlinson et al. 2017). An understanding of the CGM would resolve an aspect of the "missing baryon problem," whereby a substantial fraction of the baryons associated with halos has not been detected (Dai et al. 2010; McGaugh et al. 2010; McQuinn 2016).

Questions remain about how the CGM is distributed around galaxies and how much mass there is in the CGM (e.g., Tumlinson et al. 2017). Fast radio bursts (FRB), however, are starting to provide an unprecedented probe of the CGM, with the advent of many radio telescopes geared for this science coming online across the globe (Cordes & Chatterjee 2019; Petroff et al. 2019, 2022; Prochaska & Zheng 2019; Keating & Pen 2020). FRBs are bright (up to a few hundred jansky) transient radio pulses (typically up to a few milliseconds) of mostly extragalactic origin, and have been detected over a wide range of frequencies (100 MHz–8 GHz). As the radio waves from FRBs travel through the intervening plasma, the interaction with free electrons causes a frequency-dependent delay of their arrival time, which is proportional to the integral of the electron number density along the line of sight (with a factor of $(1+z)$ correction for cosmological lines of sight)—the dispersion measure (DM). Since most of the CGM gas is ionized, the ionized gas contributes an extra amount to the total DM along a sightline, which can be used to constrain the distribution of CGM gas (McQuinn 2014; Ravi 2019).

There are many challenges to precisely measuring the excess DM from the CGM, especially in a sample of FRBs that are not well localized. First of all, the host galaxy and local environment around the FRB can contribute from a few tens to a few hundreds of $\mathrm{pc\,cm^{-3}}$ (Kulkarni et al. 2015; Connor et al. 2016; Tendulkar et al. 2017; Yang et al. 2017; Cordes et al. 2022; Niu et al. 2022). Cosmic structures can also contribute scatter at the level of hundreds of $\mathrm{pc\,cm^{-3}}$ (McQuinn 2014; Macquart et al. 2020). If the redshifts of the FRB host and intervening galaxies can be measured, requiring arcsecond localizations, one can subtract the average cosmological contribution to the total DM, which significantly reduces the variance in the measurement. Previous theoretical works predict that $\mathcal{O}(100)$ FRBs are required to put constraints on the CGM when stacking arcsecond-localized FRBs (McQuinn 2014; Ravi 2019). However, there are approximately 20 FRBs that are sufficiently well localized to date (Petroff et al. 2022), while thousands of predominantly unlocalized FRBs have been observed, with more expected in the next few years. Without arcsecond localizations, many more FRBs are required to detect an excess DM from foreground CGMs (but see Platts et al. 2020, for constraining the Milky Way DM using a small number of transients). This paper considers this case.

We expand upon the recent work of Connor & Ravi (2021) and present a measurement of the CGM of nearby galaxies using the first FRB catalog published by the Canadian Hydrogen Intensity Mapping Experiment (CHIME) FRB project (Amiri et al. 2021). CHIME is a drift scan radio telescope operating across 400–800 MHz. The first CHIME/FRB catalog contains 535 FRBs detected between 2018 July 25 and 2019 July 1, including 18 repeating ones. While the typical localization error of 0.°2 is too large for any sophisticated analysis on the CGM, nearby ($\lesssim$100 Mpc) halos that cover even larger areas on the sky ($>0.2^2$ deg^2) make it

possible to detect the DM excess from these halo CGMs. We thus stack FRBs that intersect 10^{11}–$10^{13}\,M_{\odot}$ halos within two virial radii and measure the DM excess, with a flexible weighting function that considerably reduces the stack's variance and, importantly, downweights high-DM FRBs. We show that with our weighting scheme, having 3000 more FRBs from a CHIME data release would lead to a $>3\sigma$–4σ detection of the CGM of 10^{11}–$10^{13}\,M_{\odot}$ halos, a number that is easily achievable with CHIME in the next few years. This will open up a novel window for understanding the baryon physics in the universe, since other methods of studying the CGM, such as the thermal and kinetic Sunyaev–Zeldovich effect (Schaan et al. 2021) and halo X-ray emission (Chadayammuri et al. 2022), usually probe higher-mass ($>10^{12}$–$10^{13}\,M_{\odot}$) halos (but see Bregman et al. 2022, for a measurement of nearby halos of Milky Way size).

We note that another interesting constraint on the DM excess of the CGM comes from the repeating FRB 20200120E, which was recently localized to a globular cluster in M81 (Kirsten et al. 2022; Nimmo et al. 2023). Since the sightline does not cross the M81 disk, the DM of this FRB puts a tight upper bound on the Milky Way halo DM and M81 halo DM. With an estimate of the Milky Way disk DM of 30–40 pc cm^{-3} (Cordes & Lazio 2002; Yao et al. 2017), the sum of the two halo DMs is $\sim$50–60 pc cm^{-3}. This is broadly consistent with our measured DM excess of nearby halos.

This paper is organized as follows. Section 2 first presents our galaxy catalog and FRB sample selection. Then it describes our weighting method, the estimator of the DM excess from the CGM, and the derivation of a scheme to compare data with CGM models. Section 3 presents our measured DM excess and comparison with models, and makes forecasts for a future CHIME data release.

2. Methods

2.1. FRB Selection

We use the nonrepeaters in the CHIME FRB catalog, following Connor & Ravi (2021). Since the identified repeaters might exhibit a very different DM distribution from the nonrepeaters because the repeaters are likely younger and more energetic systems, including them may add noise to our measurements of DM excess. As in Connor & Ravi (2021), we exclude FRBs of Galactic latitudes within 5° of the Galactic plane to avoid regions where the Milky Way DM is higher such that modeling errors for this contribution can be larger. This gives a total number of 453 FRBs. We have verified that our results are not sensitive to this Galactic latitude threshold. For the FRB DM we use DM values provided by the CHIME catalog that have the Milky Way disk contribution removed using the Cordes & Lazio (2002) model. We have checked that using the Yao et al. (2017) model for the Milky Way disk DM does not change our conclusions. We do not attempt to subtract the Milky Way halo DM since it is poorly constrained (Prochaska & Zheng 2019; Keating & Pen 2020; Platts et al. 2020; Cook et al. 2023; Ravi et al. 2023), but stacking should average out the fluctuations in the Milky Way halo DM, and this DM is anticipated to be similar for all sightlines.

As in Connor & Ravi (2021), we use the galaxies in the Gravitational Wave Galaxy Catalogue (GWGC, White et al. 2011). At 40 Mpc, the angular sizes of the virial radii of 10^{11}, 10^{12}, and $10^{13}\,M_{\odot}$ halos are 0.°15, 0.°33, and 0.°70 respectively, assuming $R_{\rm vir} = 250(M/1.3\times10^{12}\,M_{\odot})^{1/3}$ kpc. We use this expression for $R_{\rm vir}$ throughout the paper. Since the typical 1σ error of CHIME localization is 0.°2, we use 10^{11}–$10^{12}\,M_{\odot}$ halos at 0.5–40 Mpc and 10^{12}–$10^{13}\,M_{\odot}$ halos at 0.5–80 Mpc for our analysis. Later on, we develop a method to account for location uncertainties when comparing CGM models. We calculate the halo masses of galaxies by converting from their stellar masses using the relation in Moster et al. (2010).[4] To estimate the galaxy stellar mass, we adopt any of four methods depending on what photometric data are available (higher priority comes first): cross-matching with NASA–Sloan Atlas catalog[5] (NSA, 4200 galaxies), *JHK*-band spectral energy distribution (SED) fitting[6] (3400 galaxies) or *K*-band mass-to-light ratio (100 galaxies), Sloan Digital Sky Survey $g-r$ color (400 galaxies). For the remaining 1900 galaxies in GWGC for which we were unsuccessful at obtaining optical or infrared photometric data, we convert their *B*-band luminosities to stellar masses by calibrating a conversion relation using the other galaxies. Among the galaxies in the NSA catalog, 1800 also have *JHK* photometric data, for which we find that our estimates of stellar mass using *JHK* bands mostly lie within a factor of 3 from the NSA stellar masses. We have verified that our main conclusions do not change if we use the *JHK* stellar masses for these galaxies instead.

For the candidate $>10^{11}\,M_{\odot}$ halos, we identify galaxy groups and remove satellite galaxies. For a given galaxy, we define it as a satellite if it lies within $1.2\,R_{\rm vir}$ of a more massive galaxy nearby in terms of their 3D distance. We do not consider M33 as a satellite of M31. Since the distances listed in GWGC have a typical error of 20%, we also test determining a satellite using the 2D projected distance and the difference in the radial velocities. We find that our results change very little if a satellite is identified by requiring that the radial velocities differ within three times the halo circular velocity instead of using the 3D distances. Our group-finding leaves 4600 10^{11}–$10^{12}\,M_{\odot}$ galaxies at 0.5–40 Mpc and 4000 10^{12}–$10^{13}\,M_{\odot}$ galaxies at 0.5–80 Mpc. We also remove five FRBs that we identify as intersecting $>10^{13}\,M_{\odot}$ halos at $<1\,R_{\rm vir}$. These more massive halos give a DM excess of $>$100–200 pc cm^{-3} (Williams et al. 2023) and so may bias our estimated DM excess for the lower-mass halos if some sightlines pass through multiple halos. However, we have checked that not removing these FRBs does not affect our conclusions. The five excluded FRBs also include two that lie close to the Virgo cluster, although their DM being only 200–400 pc cm^{-3} suggests that they originate in front of Virgo (Virgo should give an excess DM of order 1000 pc cm^{-3}, see Prochaska & Zheng 2019).

We select FRBs that intersect nearby halos out to $2\,R_{\rm vir}$ and bin them according to their $b/R_{\rm vir}$. Figure 1 shows the map of FRBs, with colors indicating the DM values, and locations of galaxies that have FRB intersections within $1\,R_{\rm vir}$. Blue and red crosses represent the centers of 10^{11}–$10^{12}\,M_{\odot}$ and 10^{12}–$10^{13}\,M_{\odot}$ halos in this sample, respectively. Ellipses of corresponding colors enclose the regions of radius $1\,R_{\rm vir}$ in R.A.–decl. coordinates. The two biggest ellipses at R.A. $<50°$ are M31 and M33. With our selections, there are 26 FRBs

[4] Different models predict similar stellar mass–halo mass relations at $z=0$, e.g., Figure 34 of Behroozi et al. (2019).

[5] Provided by Matt Wilde.

[6] We performed SED fitting using CIGALE (Boquien et al. 2019, https://cigale.lam.fr/) and find that using *JHK* bands alone provides more reliable stellar masses than using optical bands. A lot of galaxies do not have optical photometry, because we queried the NASA/IPAC Extragalactic Database (NASA/IPAC Extragalactic Database (NED) 2019) web service with astropy.

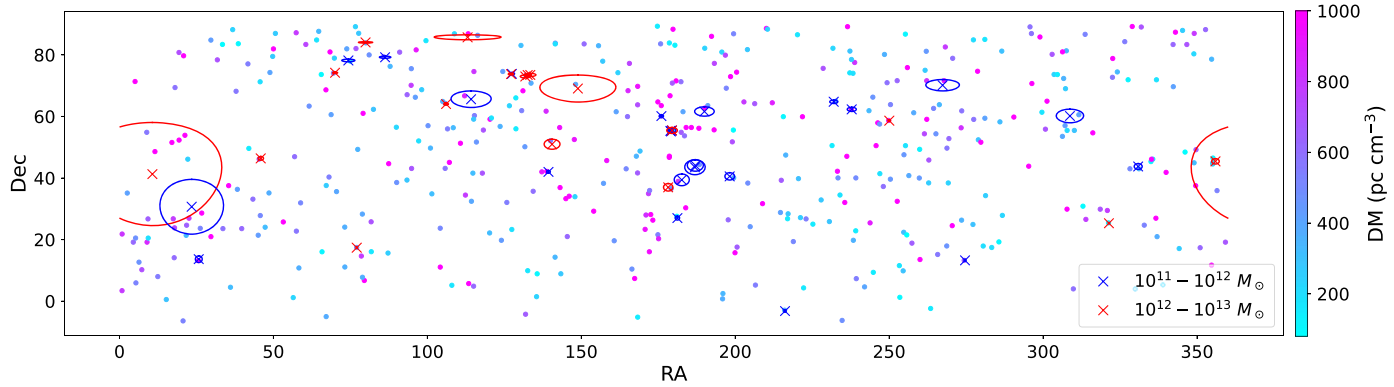

Figure 1. Locations of the CHIME catalog FRBs used in our analysis as well as of galaxies having FRB intersection with an impact parameter of $b < 1\,R_{\rm vir}$. Dots show the position of FRBs, with colors denoting their DM. Blue and red crosses illustrate the centers of 10^{11}–$10^{12}\,M_\odot$ and 10^{12}–$10^{13}\,M_\odot$ halos, respectively. Ellipses around these halos enclose the regions of radius $1\,R_{\rm vir}$ in these angular coordinates.

Table 1
Numbers of FRBs and Halos in Each Impact Parameter (b) Bin and the Measured DM Excess in Units of pc cm^{-3}

(1) b Range	(2) $N_{\rm FRB}$ 10^{11}–10^{12}	(3) $N_{\rm FRB}$ M33	(4) $N_{\rm halo}$ 10^{11}–10^{12}	(5) DM Excess	(6) $N_{\rm FRB}$ 10^{12}–10^{13}	(7) $N_{\rm FRB}$ M31	(8) $N_{\rm halo}$ 10^{12}–10^{13}	(9) DM Excess
[0, 1] $R_{\rm vir}$	26 (26–31)	6	24	71 ± 53 (18 ± 61)	30 (28–33)	16	18	69 ± 49 (96 ± 72)
[1, 1.5] $R_{\rm vir}$	31 (28–34)	5	26	87 ± 48 (78 ± 53)	38 (36–42)	22	18	-4 ± 43 (6 ± 61)
[1.5, 2] $R_{\rm vir}$	39 (32–40)	9	32	41 ± 43 (35 ± 46)	57 (49–56)	28	31	37 ± 35 (-11 ± 46)

Note. Columns 2–4: number of FRBs intersecting 10^{11}–$10^{12}\,M_\odot$ halos, number of FRBs intersecting M33, and the number of 10^{11}–$10^{12}\,M_\odot$ halos with FRB intersections. Numbers in parentheses indicate the 1σ range (16th and 84th percentiles) of the number of FRBs owing to localization uncertainties, calculated by perturbing FRB locations assuming Gaussian errors. Column 5: the estimated DM excess using Equation (5) and 1σ error, with numbers in parentheses denoting the results excluding M33. Columns 6–9: the same but for 10^{12}–$10^{13}\,M_\odot$ halos.

intersecting 24 halos with masses of 10^{11}–$10^{12}\,M_\odot$ within $1\,R_{\rm vir}$, and 30 FRBs intersecting 18 halos with 10^{12}–$10^{13}\,M_\odot$, although half of these intersections are with M31. Among the FRBs selected, three pass through both low-mass and high-mass halos, giving 53 in total. Table 1 lists the numbers of FRBs and halos falling in impact parameter bins of [0, 1], [1, 1.5], and [1.5, 2] $R_{\rm vir}$. The numbers in parentheses in this table represent the 1σ error on these numbers owing to localization uncertainties, obtained by perturbing FRB locations assuming Gaussian errors.[7] If an FRB falls into multiple radial bins owing to intersections with different halos, we only count this FRB once, grouping it with the halo it intersects at the smallest impact parameter. We have tested that counting the halo twice does not change our results.

2.2. An Estimator of DM Excess

We aim to examine whether the FRBs with impact parameter $b < 2\,R_{\rm vir}$ exhibit a statistically significant excess DM over the full sample of FRBs. A simple estimator for the DM excess is the mean DM of the sample minus the mean of all CHIME FRBs. However, since the number of FRBs with halo intersections is small, one or two FRBs with high DM can significantly affect the sample mean DM. For a sample size of 20, one FRB with DM $=$ 2000 pc cm^{-3} contributes 100 pc cm^{-3} to the sample mean, and the CHIME FRBs have a high-DM tail of DM $\gtrsim$ 1500 (see the black histogram in Figure 2; hereafter we omit the unit of DM, pc cm^{-3}). An unweighted mean is thus not an ideal estimator for the DM excess because high DM bursts add to the variance of the estimated DM excess and bias it. Therefore, instead of calculating the sample mean DM, we compute a weighted-average DM where we downweight contributions from high-DM FRBs using a flexible weighting function

$$w(\mathrm{DM}) \propto \exp\left(-(\mathrm{DM}/\alpha)^{\beta}\right), \tag{1}$$

where α and β shape how quickly the weight cuts off. Hereafter we assume that the weights are already normalized so that the sum of weights equals unity. For a subsample of FRBs intersecting CGMs, a simple statistical measure (which we will improve below) for the DM excess is

$$\widetilde{\delta\mathrm{DM}} = \sum_{i\in\mathcal{I}} w(\mathrm{DM}_i)\mathrm{DM}_i - \overline{\mathrm{DM}}, \tag{2}$$

where i denotes the indices of FRBs, $\mathcal{I}$ is the subset of $N_{\rm DM}$ FRBs with CGM intersections, and

$$\overline{\mathrm{DM}} = \sum_{i\in\mathrm{CHIME}} w(\mathrm{DM}_i)\mathrm{DM}_i \tag{3}$$

is the weighted mean DM of the whole CHIME sample. This downweighting is a major difference of our work from Connor & Ravi (2021), who used uniform weighting.[8] Optimizing our

[7] We note that the error bars on the number of FRBs in a bin are likely asymmetric around the number calculated using the maximum likelihood localization. This occurs because some FRBs fall on the edge of halos.

[8] A counterargument to downweighting is that the high-DM FRBs, which presumably originate from halos at higher redshift, should encounter more CGMs along the line of sight so can be upweighted for measuring the DM excess of the CGM. However, since we want to study the CGM of nearby halos, in principle we just need the FRBs that originate right behind these halos. High-DM FRBs that go through more CGMs will not contribute to our measurements and will only add noise to our estimates.

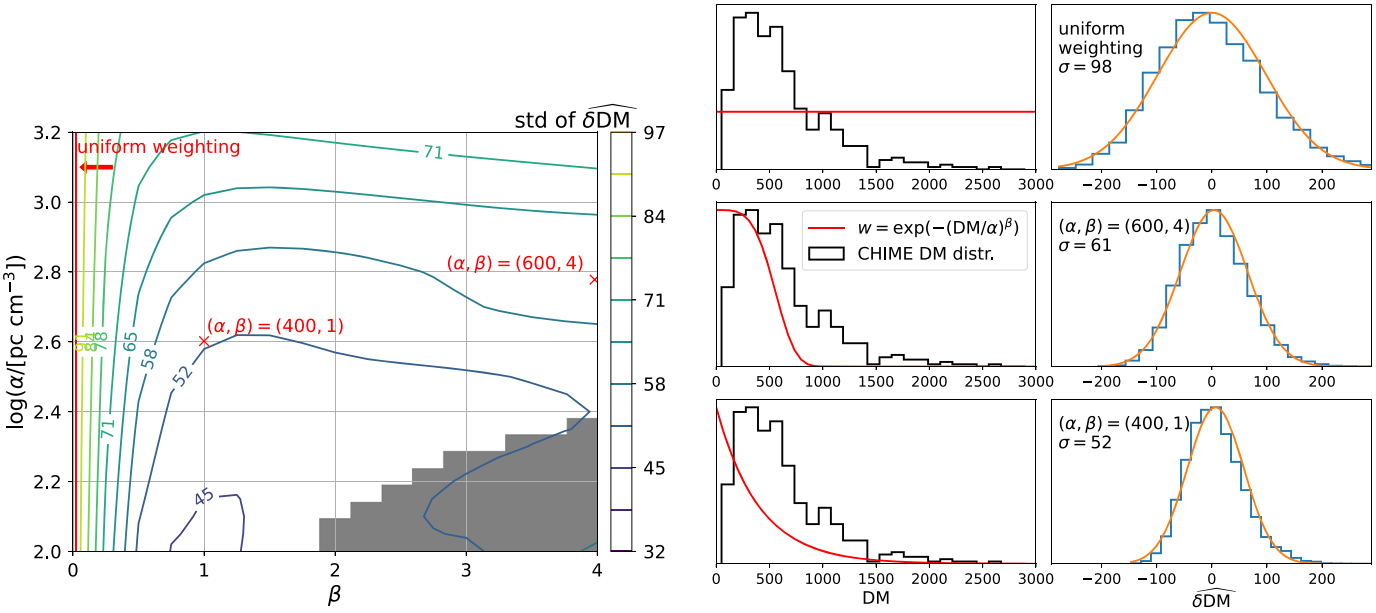

Figure 2. Left panel: contours of the standard deviation (std) of the weighted-average DM as a function of the parameters of our weight function α and β (see Equation (1)), obtained by randomly sampling 20 FRBs from the CHIME DM distribution. The gray shaded region represents α, β values that can suppress all sampled DM values. The line at $\beta = 0$ and red crosses indicate the weighting functions we examine in the right panels: uniform weighting, $(\alpha, \beta) = (600, 4)$, and $(\alpha, \beta) = (400, 1)$. Middle panels: the black lines show the DM histogram of the CHIME FRBs, and red lines represent the corresponding weighting functions in arbitrary units. Right panels: histogram of the excess weighted-average DM (Equation (5)) for different values of α, β and uniform weighting (blue lines). Orange lines represent Gaussian fits to the histograms. Also quoted are the standard deviations of the weighted-mean DM. All DMs are in units of pc cm^{-3}.

weighting function by minimizing the estimated DM in the two-dimensional (α, β) space allows us to detect a DM excess with added precision.

For a nonlinear weighting function, the simple estimator of the DM excess given by Equation (2) is a biased estimate of the true DM excess, which we will revise below. To see this, if we artificially add a DM excess δDM to an arbitrary array of DM values, we have

$$\begin{aligned}\widetilde{\delta\mathrm{DM}} &= \sum_i w(\mathrm{DM}_i + \delta\mathrm{DM})(\mathrm{DM}_i + \delta\mathrm{DM}) \ - \ \overline{\mathrm{DM}} \\ &= \sum_i w(\mathrm{DM}_i + \delta\mathrm{DM})(\mathrm{DM}_i + \delta\mathrm{DM}) \\ &\quad - \sum_i w(\mathrm{DM}_i)\mathrm{DM}_i \\ &= \left[\sum_i w(\mathrm{DM}_i + \delta\mathrm{DM})\mathrm{DM}_i - \sum_i w(\mathrm{DM}_i)\mathrm{DM}_i\right] \\ &\quad + \delta\mathrm{DM},\end{aligned}$$

where in each summation the weights are normalized to sum to 1. One can see that if $\beta > 1$, $\widetilde{\delta\mathrm{DM}} < \delta\mathrm{DM}$; if $0 < \beta < 1$, then $\widetilde{\delta\mathrm{DM}} > \delta\mathrm{DM}$. Only when $\beta = 1$ do we get $\widetilde{\delta\mathrm{DM}} = \delta\mathrm{DM}$. To correct for this offset, we thus define a bias factor

$$f = \widetilde{\delta\mathrm{DM}}/\delta\mathrm{DM}, \tag{4}$$

which we find is nearly independent of the DM excess for $\delta\mathrm{DM} < 200$, a limit that is easily satisfied in models for the foreground CGMs of galactic halos. This independence of f is convenient as it means that the correction does not depend on the true excess. Our revised unbiased estimator for the DM excess is thus

$$\widehat{\delta\mathrm{DM}} = \widetilde{\delta\mathrm{DM}}/f = \left[\sum_{i\in\mathcal{I}} w(\mathrm{DM}_i)\mathrm{DM}_i - \overline{\mathrm{DM}}\right]/f, \tag{5}$$

which we will use to measure the DM excess of CHIME FRBs intersecting halos.

For self-consistency, one can easily verify that for the range of DM excess that we are interested in here ($\widehat{\delta\mathrm{DM}} \lesssim 200$) and for the α, β ranges that we adopt for CHIME FRBs (see Section 3.1), Equation (5) gives the same DM excess estimate as iteratively solving

$$\widehat{\delta\mathrm{DM}} = \sum_{i\in\mathcal{I}} w(\mathrm{DM}_i - \widehat{\delta\mathrm{DM}})\ \mathrm{DM}_i - \overline{\mathrm{DM}}, \tag{6}$$

where in each iteration the weights $w(\mathrm{DM}_i - \widehat{\delta\mathrm{DM}})$ have to be normalized. If one is interested in much larger DM excess or FRBs encountering multiple halos, the correction factor f should be recalibrated according to the proper choice of the weighting function.

2.3. Goodness of Fit of CGM Models

The above gives a way of calculating a statistical average of the DM excess for FRBs intersecting CGMs. We now extend Equation (6) to allow each FRB to have a different DM excess that is predicted by some CGM models, so that we can derive a metric to compare models with the data. Suppose we are in the limit of a very large number of FRBs, although with imprecise localization so the hosts are unknown. We expect the following relation to hold for the subsample ($\mathcal{I}$) of FRBs that have CGM

intersections:

$$\sum_{i\in\mathcal{I}}[\mathrm{DM}_i - \delta\mathrm{DM}_i]w(\mathrm{DM}_i - \delta\mathrm{DM}_i) = \overline{\mathrm{DM}}. \quad (7)$$

Here, unlike Equation (6), $\delta\mathrm{DM}_i = \delta\mathrm{DM}_i(b, M)$ models the excess DM from intervening CGM in terms of the impact parameter b and halo mass M of each foreground galaxy (and not necessarily just one halo despite our notation).

We aim to find the model for $\delta\mathrm{DM}_i$ that best describes the data. We therefore define a measure for the goodness of fit

$$\xi^2 = \left(\left\{\sum_{i\in\mathcal{I}}[\mathrm{DM}_i - \delta\mathrm{DM}_i]w(\mathrm{DM}_i - \delta\mathrm{DM}_i)\right\} - \overline{\mathrm{DM}}\right)^2. \quad (8)$$

We can also take the expectation value of ξ^2 by randomly sampling the same number of intersections from the full DM distribution:

$$\langle\xi^2\rangle = \left\langle\left(\sum_i w(\mathrm{DM}_i)\mathrm{DM}_i - \overline{\mathrm{DM}}\right)^2\right\rangle, \quad (9)$$

where the summation goes over the desired number of FRBs N_{DM}. Since $\langle\xi^2\rangle$ is like the squared variance of the sample mean DM, it scales with N_{DM} as $\langle\xi^2\rangle \propto N_{\mathrm{DM}}^{-1}$.

Our formalism still holds when dividing the FRBs into impact parameter bins based on their b/R_{vir} values, as long as there are enough FRBs in a bin. For each radial bin j, we can calculate the χ^2 statistic by dividing ξ^2 by $\langle\xi^2\rangle$ in that bin:

$$\chi_j^2 = \frac{\xi_j^2}{\langle\xi^2\rangle_j}(|\boldsymbol{b}|), \quad (10)$$

which is a function of the set of impact parameters $\boldsymbol{b}$. Summing these over radial bins gives the total:

$$\chi^2 = \sum_j \chi_j^2. \quad (11)$$

The above is the procedure without accounting for localization error. However, for some of our intersections, the localization is comparable to the halo virial radius. To take account of the localization uncertainties, we calculate the marginalized χ^2 value of bin j:

$$\exp(-\chi_j^2/2) = \int \exp\left(-\frac{1}{2}\frac{\xi_j^2}{\langle\xi^2\rangle_j}(|\boldsymbol{b}|)\right) P(\boldsymbol{b})\, \mathrm{d}\boldsymbol{b}. \quad (12)$$

The total χ^2 is

$$\exp(-\chi^2/2) = \int \exp\left(-\frac{1}{2}\sum_j \frac{\xi_j^2}{\langle\xi^2\rangle_j}(|\boldsymbol{b}|)\right) P(\boldsymbol{b})\, \mathrm{d}\boldsymbol{b}. \quad (13)$$

We will calculate these χ^2 values for different CGM models in Section 3.3.

3. Results

3.1. Choice of the Weighting Function Parameters

Before we measure the DM excess from intervening CGMs using the CHIME FRB catalog, we first determine the best values of α, β to use in our weighting function (Equation (1)). We thus examine how much reduction in the variance of the weighted-average DM our weighting function can give. To this end, we created a mock FRB catalog of size 10^5 that has the same DM distribution as the CHIME catalog. We then randomly sample N_{DM} FRBs from this mock catalog and for each sample calculate $\widehat{\delta\mathrm{DM}}$ using Equation (5) for a range of α, β values. We repeat this step 10,000 times and compute the standard deviation (std) of $\widehat{\delta\mathrm{DM}}$ for each α, β.

The left panel of Figure 2 shows contours of the std of $\widehat{\delta\mathrm{DM}}$ as a function of α, β, obtained by randomly sampling $N_{\mathrm{DM}} = 20$ FRBs from the CHIME DM distribution. Twenty is chosen to roughly match the number of CHIME FRBs with halo intersections, although we find that the contours of the std of $\widehat{\delta\mathrm{DM}}$ remain mostly unchanged when assuming different N_{DM}, such as $N_{\mathrm{DM}} = 100$. The gray shaded region represents α, β values that can lead to all zero weights to machine precision, for at least one time out of the 10,000 times of random sampling (so that only one FRB receives any weight). The best estimator for mean DM when sampling 20 FRBs seems to be given by values near $(\alpha, \beta) = (100, 1)$ that lead to a factor of 2.2 in the estimator std relative to uniform weighting, but such a weighting falls off exponentially above the low value of DM ~ 100, selecting the few sightlines with the smallest DM. Therefore, the minimum variance estimator is close to selecting the minimum DM—for many distributions the minimum value in the DM array converges faster than the mean. However, the minimum DM is only useful for our estimate of the DM excess when there is intervening CGM. If the minimum-DM FRB actually originates from a nearby halo (e.g., the low-DM FRBs in Bhardwaj et al. 2021a, 2021b) instead of intervening from further away, the minimum DM becomes problematic. We thus explore $(\alpha, \beta) = (600, 4)$ and $(400, 1)$, which—while giving substantial weight to about half of the FRBs—still give a reduction by factors of 1.6 and 2 of the standard deviation relative to an unweighted estimator, respectively, and just modestly larger variances than the minimum variance $(\alpha, \beta) = (100, 1)$ of a 2.2 reduction.[9]

The black lines in the middle panels of Figure 2 illustrate the DM histogram of the CHIME FRBs, and red lines represent these weighting functions in arbitrary units. From top to bottom we use uniform weighting, $(\alpha, \beta) = (600, 4)$, and $(\alpha, \beta) = (400, 1)$. Using $(\alpha, \beta) = (600, 4)$ has a much stronger cutoff at high DM values, leading to 20%–30% of the CHIME DM distribution contributing negligibly. The right panels of Figure 2 show the histograms of $\widehat{\delta\mathrm{DM}}$ by randomly sampling 20 FRBs from mocks. Blue lines illustrate the histograms, and the orange lines represent Gaussian fits to the histograms. Also quoted are the standard deviations of $\widehat{\delta\mathrm{DM}}$. Since $(\alpha, \beta) = (400, 1)$ gives a slightly more skewed distribution of the weighted-mean DM with a high-value tail, by default we use $(\alpha, \beta) = (600, 4)$, but we have verified that $(\alpha, \beta) = (400, 1)$ yields very similar stacked DM excesses and conclusions.

[9] The bias factor f of the estimator with $(\alpha, \beta) = (600, 4)$ is 0.65, while $(400, 1)$ is unbiased.

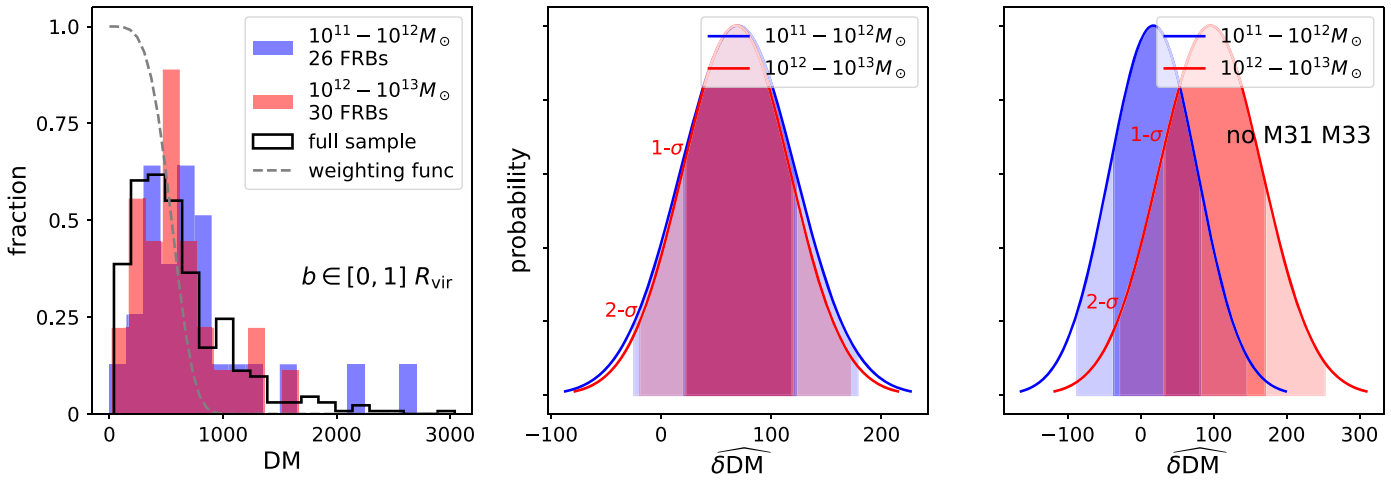

Figure 3. Statistics of CHIME FRBs that intersect nearby 10^{11}–$10^{12}\,M_\odot$ (blue) and 10^{12}–$10^{13}\,M_\odot$ (red) halos within $1\,R_{\rm vir}$. Left panel: the blue and red histograms show the DM distributions of the 26 and 30 FRBs intersecting the smaller and larger halo mass bins, respectively. The black line illustrates the DM distribution of the full CHIME sample. The gray dashed line represents our weighting function in arbitrary units, which is effectively multiplied by the DM distribution to calculate the stacked DM. Middle panel: the blue and red lines represent the likelihood of our estimator $\widehat{\delta \rm DM}$ with $(\alpha, \beta) = (600, 4)$ for the whole CHIME sample, where the central value is our measurement—the estimator applied to the observational data—and the Gaussian probability distribution function is calculated by randomly sampling the CHIME DM distribution with 26 and 30 FRBs respectively. Shaded regions show the 1σ and 2σ bounds of the distributions. Right panel: the same as the middle panel, except that we have excluded FRBs that intersect M31 and M33, which results in 20 FRBs intersecting 10^{11}–$10^{12}\,M_\odot$ halos and 15 intersecting 10^{12}–$10^{13}\,M_\odot$ ones.

3.2. The Measured DM Excess

Using the FRBs that intersect halos, we measure their excess DM by using the estimator given by Equation (5) with $(\alpha, \beta) = (600, 4)$. The left panel of Figure 3 shows the DM distributions of the 26 FRBs that intersect 10^{11}–$10^{12}\,M_\odot$ halos (blue) within $1\,R_{\rm vir}$, and the 30 FRBs intersecting 10^{12}–$10^{13}\,M_\odot$ halos (red). The black line represents the DM distribution of the whole CHIME sample. The gray dashed line represents our weighting function. The middle panel shows the probability distributions of the measured DM excess, centered on the solution of Equation (5) with the std determined by randomly sampling 26 (blue line) and 30 (red line) FRBs from the CHIME DM distribution respectively. The shaded regions indicate the 1σ and 2σ bounds of the distributions. The estimated DM excess is similar for both halo ranges, and the similar number of FRBs in each group leads to similar error bars. The excess DM of both halo groups is detected at about 1.5σ. Owing to the large extent of M31 and M33 on the sky, we also performed our analysis without the FRBs intersecting these galaxies. This gives 20 FRBs intersecting 10^{11}–$10^{12}\,M_\odot$ halos and 15 intersecting 10^{12}–$10^{13}\,M_\odot$ ones. The right panel shows the distributions of the excess DM when excluding M31 and M33. This exclusion lowers the estimated DM excess of the lower-mass group but raises that of the higher-mass one, and the error bars of both groups are enlarged by a factor of $\sim$1.3. While the DM excess from 10^{12}–$10^{13}\,M_\odot$ halos can still be detected at 1.3σ level, an insignificant excess in the 10^{11}–$10^{12}\,M_\odot$ mass bin is statistically preferred.

Our $\lesssim 1.5\sigma$ detection of the foreground CGM is less significant than the $>2\sigma$ detection in Connor & Ravi (2021), even though the std of our weighted estimator is a factor of two smaller than their unweighted one. However, there are two FRBs with DM > 2000 intersecting 10^{11}–$10^{12}\,M_\odot$ halos (left panel of Figure 3). Without a weighting function, these FRBs raise the sample mean DM by over 100, for a sample size of 30. This likely leads to the t-test returning $p < 0.05$ in Connor & Ravi (2021).

We performed the same analysis on the DM excess of FRBs intersecting halos within impact parameters of 1–1.5 $R_{\rm vir}$ and 1.5–2 $R_{\rm vir}$. We find that the FRBs intersecting 10^{11}–$10^{12}\,M_\odot$ halos continue to show a DM excess at $\gtrsim 1\sigma$ level in these more extended radial bins, while the 10^{12}–$10^{13}\,M_\odot$ halos no longer show a DM excess there. Figure 4 summarizes our stacking results. Dots with error bars show the measured DM excess as a function of $b/R_{\rm vir}$ assuming constant DM excess in each radial bin. Left and right panels illustrate results for the 10^{11}–$10^{12}\,M_\odot$ and 10^{12}–$10^{13}\,M_\odot$ halos, respectively. The black and gray colors indicate inclusion of all halos and exclusion of M31 and M33, respectively. The values of b used to plot the measurements are the weighted average of b in each radial bin, with the weights given by our weighting function and the DM. As a reference for the expected DM excess, this figure also shows the radial DM profiles for a model in which the CGM gas traces the Navarro–Frenk–White (NFW) profile and another where it is distributed as a top-hat model with radius of $2\,R_{\rm vir}$ (STH2). Our DM excess measurements are largely consistent with the model predictions. Both models are discussed in what follows.

3.3. Comparison with CGM Models

Since our constraints are in the ballpark of the expected DM excess of the CGM, it is possible that they already rule out some CGM models. Given a model of the CGM, the radial profile of DM around a sample of halos has a one-halo term owing to the gas surrounding these halos themselves, and also a rather flat two-halo term coming from the overlapping of gas from other halos. We use the DM radial profiles calculated using the CGMBrush algorithm (Williams et al. 2023) for our χ^2 calculation. This algorithm subtracts the dark matter associated with each halo in an N-body simulation and then adds on different models for the

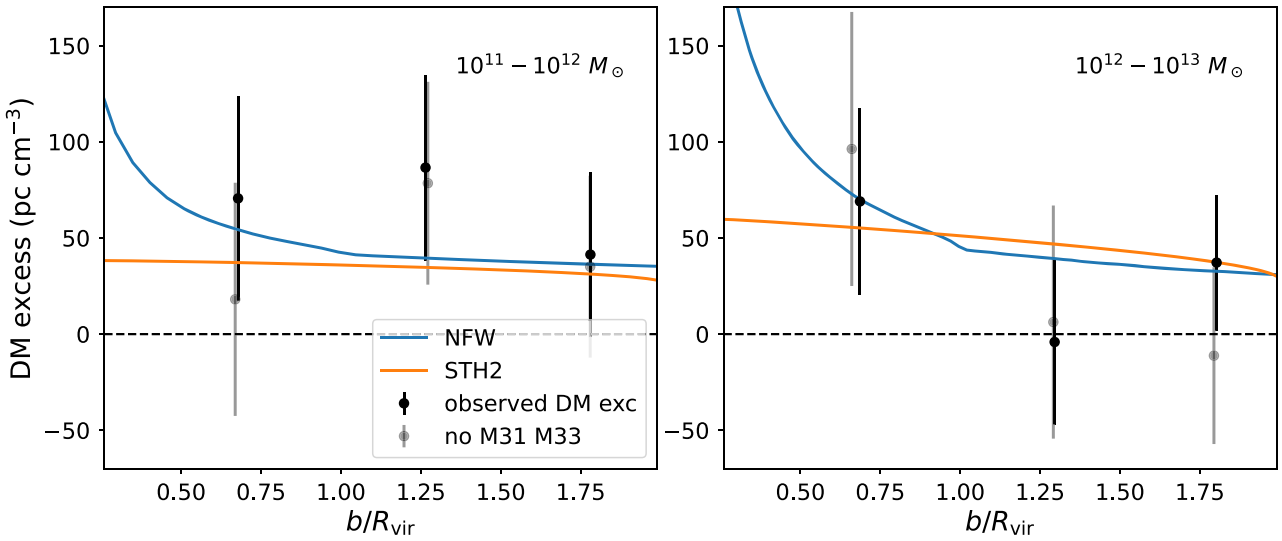

Figure 4. The measured and model-predicted DM excess as a function of impact parameter at different impact parameters b to the foreground halo. Left and right panels show our results for the 10^{11}–$10^{12}\,M_\odot$ and 10^{12}–$10^{13}\,M_\odot$ halos, respectively. Black points with error bars illustrate the observed DM excess including all halos, and the gray points are those excluding M33 (left panel) or M31 (right panel). As a reference for the expected signal amplitude, the blue and orange lines show the radial DM profiles in the NFW-tracing and the $2\,R_{\rm vir}$ spherical top-hat (STH2) models for the CGM gas, respectively (see Section 3.3). These models are calculated assuming halo masses of $4\times10^{11}\,M_\odot$ (left) and $4\times10^{12}\,M_\odot$ (right).

distribution of the gas associated with that halo. It assumes that gas outside halos traces the dark matter.[10] Using these models for the DM excess, we calculate χ^2 values using Equations (8) and (12) for FRBs in each of the three radial bins [0, 1], [1, 1.5], and [1.5, 2], in units of $R_{\rm vir}$. To speed up the calculation, we restrict to using FRBs that lie within $(2\,R_{\rm vir}+3\times0.^\circ2)$ of galaxies, where $0.^\circ2$ is the typical localization error of CHIME. As mentioned in Section 2.1, we count an FRB only once if it intersects multiple halos. Counting galaxy–FRB pairs instead leads to somewhat larger $\Delta\chi^2$, but with differences smaller than 1–2. To evaluate the high-dimension integral on the right-hand side of Equation (12) or Equation (13), we draw from a 2D Gaussian for the location of each FRB on the sky plane so that the draws trace $P(\boldsymbol{b})$ and sum up 10^4 realizations for a Monte Carlo evaluation.

We perform this χ^2 calculation for the STH2 model of the CGM where the gas is distributed as a top hat with radius of $2\,R_{\rm vir}$ and the NFW model. These extreme models roughly bound the DM excess predicted by the more realistic models in Williams et al. (2023). The STH2 model has only an eighth of the halo-associated baryons within $1\,R_{\rm vir}$, whereas the NFW contains all of them within $1\,R_{\rm vir}$. Indeed, owing to its diffuseness, we find that the STH2 DM excess is shaped at most radii by the two-halo term and not the halo profile. Figure 4 illustrates DM excess as a function of $b/R_{\rm vir}$ predicted by the NFW (blue lines) and the STH2 (orange lines) models. These illustrative curves in the left and right panels assume halo masses of $4\times10^{11}\,M_\odot$ and $4\times10^{12}\,M_\odot$ respectively, roughly the mean of our two halo samples. Despite these two profiles having very different assumptions for the halo-associated baryons, these models give similar predictions outside $0.5\,R_{\rm vir}$, with DM differences smaller than 50 because of the large two-halo excess that depends weakly on the halo gas profiles. Our sample contains only seven and four FRBs intersecting the small and large halo mass bins with $b<0.5\,R_{\rm vir}$ respectively. The STH2 model predicts a flat DM excess of 30–50 at 0.5–1 $R_{\rm vir}$ for the 10^{11}–$10^{12}\,M_\odot$ halos, and 50–80 for the 10^{12}–$10^{13}\,M_\odot$ halos. The NFW model produces 30–50 pc cm^{-3} higher DM excess than the STH2 model. The two-halo term is about 30–50 for both halo mass bins outside $1\,R_{\rm vir}$. Because the DM differences among models are only $\lesssim$50, we expect the χ^2 values of these two models (and other models in Williams et al. 2023) to differ only at $<1\sigma$ level.

Table 2 lists the χ^2 values as well as their differences, $\Delta\chi^2$, in each radial bin. It also lists the total χ^2 summing over all bins. By default, we calculate χ^2 by marginalizing localization errors, but we show the χ^2 computed using maximum likelihood localization in parentheses (i.e., assuming $P(\boldsymbol{b})$ is a δ-function at the best-fit value).[11] Not marginalizing over localization errors generally changes the results at the $<1\sigma$ level, but in some cases the differences are somewhat larger, showing that accounting for positional errors is important. The $\Delta\chi^2$ values are calculated by subtracting χ^2 of the STH2 or NFW model from that of the model with no DM excess. We have also verified that further dividing the radial bins (but keeping at least 15–20 FRBs in a bin) does not affect the $\Delta\chi^2$ values. With three radial bins we would expect total $\chi^2\sim3$, and the models produce a slight overfit of total $\chi^2\sim1.5$.

The χ^2 in all radial bins of the 10^{11}–$10^{12}\,M_\odot$ halos disfavors the model with no DM excess at $\sqrt{\Delta\chi^2}\approx1\ \sigma$ level, although the significance level drops when excluding M33. The total χ^2 of NFW and STH2 models considering all bins is smaller than that of the case with no DM excess by 2–5, regardless of marginalizing over the localization uncertainties or using maximum likelihood localization. Thus the

[10] To compute the total DM excess for an FRB for the few sightlines that have multiple intersections, we first sum up the one-halo terms from all the nearby 10^{11}–$10^{13}\,M_\odot$ halos that this FRB can intersect along its sightline. We compute an average two-halo term using these halos and add to the total excess DM, since an FRB may intersect multiple halos at $>1\,R_{\rm vir}$. It perhaps makes the most sense to take the maximum value of the two-halo terms if the intersecting halos are within several impact parameters, and to sum the two-halo terms if halos are further apart than several impact parameters. However, the exact algorithm does not affect our results by $\Delta\chi^2>1$.

[11] We note that technically $\chi^2\geqslant\sum_j\chi^2_j$, with equality achieved when $P(\boldsymbol{b})$ is a delta function. This is why the total χ^2 differences are larger than summing up the $\Delta\chi^2$ values in individual bins.

Table 2
χ^2 and $\Delta\chi^2$ Values of Different Models in Each Impact Parameter (b) Bin, for the 10^{11}–$10^{12}\,M_\odot$ (upper) and 10^{11}–$10^{12}\,M_\odot$ (lower) Halos

(1) 10^{11}–$10^{12}\,M_\odot$	(2) χ^2 no DM exc.	(3) $\Delta\chi^2$ no DM exc. – STH2	(4) $\Delta\chi^2$ no DM exc. – NFW	(5) $\Delta\chi^2$ no M33 no DM exc. – NFW
[0, 1] $R_{\rm vir}$	2.3 (1.1)	1.6 (1.0)	1.6 (0.7)	0.5 (0.0)
[1, 1.5] $R_{\rm vir}$	1.7 (4.1)	1.2 (3.2)	1.2 (3.0)	0.8 (2.3)
[1.5, 2] $R_{\rm vir}$	1.3 (0.8)	0.8 (0.8)	0.9 (0.8)	0.7 (0.5)
Total	6.3 (6.0)	4.5 (5.0)	4.6 (4.5)	2.6 (2.8)
10^{12}–$10^{13}\,M_\odot$	χ^2 no DM exc.	$\Delta\chi^2$ no DM exc. – STH2	$\Delta\chi^2$ no DM exc. – NFW	$\Delta\chi^2$ no M31 no DM exc. – NFW
[0, 1] $R_{\rm vir}$	1.7 (2.0)	1.5 (1.9)	1.4 (1.9)	1.6 (1.9)
[1, 1.5] $R_{\rm vir}$	0.3 (0.0)	−0.7 (−1.3)	−0.5 (−1.0)	−0.6 (−0.5)
[1.5, 2] $R_{\rm vir}$	1.0 (1.2)	0.8 (1.2)	0.8 (1.2)	−1.1 (−1.2)
Total	3.1 (3.2)	1.8 (1.8)	1.7 (2.2)	−0.3 (0.1)

Note. In Column (1) Total is the total χ^2 considering all bins. For each χ^2 value we list the χ^2 values by marginalizing over localization uncertainties, and the number in parentheses shows the χ^2 obtained by using the maximum likelihood localization. Column (2): χ^2 of the model with no DM excess. Columns (3) and (4): $\Delta\chi^2$ of no DM excess minus the 2 $R_{\rm vir}$ spherical top-hat model (STH2) and the NFW model. Column (5): $\Delta\chi^2$ of no DM excess minus the NFW model, excluding M33 or M31.

significance that a DM excess is preferred over no excess ranges from 1.4σ to 2.2σ. The 10^{12}–$10^{13}\,M_\odot$ halos, on the other hand, favor a DM excess only in the [0, 1] $R_{\rm vir}$ bin and cannot distinguish any models for the larger impact parameter bins. The $\Delta\chi^2$ values are consistent with our results in Figure 3. Finally, the χ^2 of the STH2 and NFW models are very similar, as anticipated, and so not distinguishable by the data.

3.4. How Many FRBs are Needed to Get a Significant Detection of DM Excess?

Thus, we have found a marginal detection of an excess DM when stacking on foreground halos, but the data set of 453 FRBs is insufficient to distinguish between realistic CGM models. Larger samples are of course required to get a more significant detection of a given DM excess of 50–100—the anticipated DM excess for the CGM of 10^{11}–$10^{13}\,M_\odot$ halos—and this is also the difference between viable models for $b < 0.5\,R_{\rm vir}$. Since we currently get an error bar in DM of 50 with ≈30 intersections, we anticipate that the error bar scales with the number of intersections as $\sigma_{\rm DM} = 50\sqrt{30/N_{\rm DM}}$. With 200 intersections then $\sigma_{\rm DM} = 20$; this many intersections would require about 3000 FRBs in the next CHIME data release.

Currently the number of sightlines passing through halos at $<0.5\,R_{\rm vir}$ is too small, but this is the region where viable models for the CGM gas profile differ the most. With about 10^4 more FRBs from CHIME, the number of intersections with 10^{11}–$10^{13}\,M_\odot$ halos at $b < 0.5\,R_{\rm vir}$ will reach ∼200. Such a sample would be able to put novel constraints on CGM models.

4. Conclusions

We have measured the DM excess owing to the CGM of 10^{11}–$10^{13}\,M_\odot$ halos at <80 Mpc using the CHIME/FRB first data release. To this end, we have developed a weighted stacking scheme to reduce the variance of the observed DM distribution and to lower the bias of high-DM FRBs on the sample mean DM. With 20–30 FRBs intersecting 10^{11}–10^{12} and 10^{12}–$10^{13}\,M_\odot$ halos at $<1\,R_{\rm vir}$, we find that the DM excess of these halo groups can be detected at 1σ–2σ. We also tentatively detect a DM excess at impact parameters of 1–2 $R_{\rm vir}$ for 10^{11}–$10^{12}\,M_\odot$ halos, but not for the 10^{12}–$10^{13}\,M_\odot$ halos. With more FRB data from CHIME coming in the near future, each stack's signal-to-noise ratio will continue to improve with an error of $\sigma_{\rm DM} = 50\sqrt{30/N_{\rm DM}}$ pc cm^{-3}, where $N_{\rm DM}$ is the number of intersections (which was approximately 30 in our stacks).

We have also calculated the likelihood of different CGM models given the CHIME FRB data. All models are favored by the data at 1.4σ–2.2σ over a model with no DM excess, consistent with our measurements of a DM excess. We find that viable models for the CGM gas distribution produce DM differences smaller than 50 outside $0.5\,R_{\rm vir}$ because of the importance of the two-halo term around 10^{11}–$10^{13}\,M_\odot$ halos. Owing to the paucity of intersections at these impact parameters, a large increase in the number of FRBs to at least 10,000 would be needed to discriminate between viable CGM model with our method that stacks on nearby galaxies.

In the next few years, our weighted stacking method will continue to be a valuable tool to detect and measure the CGM of nearby halos as more data from CHIME arrive, especially for the relatively low-mass ones as we considered here, whose CGM is hard to probe in any other way. For a different data set with a different DM distribution, one can recalibrate a weighting function suitable for the shape of the distribution and geared more toward measuring the halos of interest. With new surveys launching that aim to observe FRBs with arcsecond localizations, other methodologies may provide better constraints on the CGM gas profile. For instance, the Canadian Hydrogen Observatory and Radio-transient Detector (CHORD, Vanderlinde et al. 2019) will receive >20 bursts per day, with the goal of providing milliarcsecond localization accuracy of FRBs with very long baseline interferometry. DSA-2000 will also start observing ∼75% of the full sky with arcsecond spatial resolution (Hallinan et al. 2019). The BURSTT project is expected to detect and localize ∼100 bright nearby FRBs per year (Lin et al. 2022). Once localized to a galaxy, the mean cosmic dispersion to a redshift can be removed from each FRB, which will dramatically reduce the noise in the stack, allowing constraints with just hundreds of bursts (McQuinn 2014; Williams et al. 2023). It might even be possible to forward-model each component (intergalactic, Milky Way, host galaxy) of the FRB DM instead of performing

weighted stacking. In particular, the intergalactic contribution might be modeled with a reconstruction of the underlying density field (e.g., Burchett et al. 2020; Lee et al. 2022). This may be particularly useful when dealing with FRBs that originate way beyond the local universe so that they have multiple halo intersections and have large total DM (e.g., FRBs from $z > 0.1$, Lee et al. 2022), which is a regime where our weighted stacking becomes less powerful. The improved angular resolution of these surveys will also allow stacking on galaxies that are further away than in this study. Another interesting related direction is to constrain the fraction of cool ionized gas via scattering and lensing of FRBs (Prochaska et al. 2019; Vedantham & Phinney 2019).

We thank Ian Williams for providing the CGMBrush profiles, Matt Wilde for offering the NSA galaxy catalog, and Bryan Gaensler, Yakov Faerman, Ue-Li Pen, and Sandro Tacchella for useful discussions. We acknowledge support from NSF award AST-2007012. This research has made use of the NASA/IPAC Extragalactic Database (NED), which is operated by the Jet Propulsion Laboratory, California Institute of Technology, under contract with the National Aeronautics and Space Administration.

Software: astropy (Astropy Collaboration et al. 2013), CIGALE (Boquien et al. 2019), PATH (Aggarwal et al. 2021).

Appendix
Possibility of FRBs Originating from Nearby Halos

While we have implicitly assumed that all the FRBs used in this work should originate from halos further away than 40–80 Mpc, it is likely that some FRBs may come from nearby halos, especially low-DM (DM $\lesssim$ 100) ones (Bhardwaj et al. 2021a, 2021b). Even for FRBs with DM of several hundred, it is not unlikely that they are from nearby galaxies because the host DM may well be a few hundred (Table 2 of Cordes et al. 2022).

To address this issue, we ran the Probabilistic Association of Transients to Hosts (PATH) code[12] to determine which FRBs might originate from <80 Mpc galaxies (Aggarwal et al. 2021). PATH calculates the probability that an extragalactic transient source is associated with a candidate host galaxy using the Bayes' rule. For each FRB, we take all <80 Mpc galaxies in GWGC that lie within three times the R.A.–decl. error bars of the FRB to be the candidates that the FRB can be associated with. Instead of using the "inverse" prior that assumes brighter galaxies have higher probabilities, we adopt a uniform prior. We assume that the distribution of FRBs around galaxies follows an exponential profile, where the size of the exponential function is given by the tabulated major and minor diameters of galaxies in GWGC. PATH then integrates over the FRB localization ellipse, and finds the galaxy with a >0.95 posterior to be the most likely host of the FRB. It does not take into account the FRB DM, however.

For the 26 (30) FRBs that we find to pass through nearby 10^{11}–$10^{12}\,M_{\odot}$ (10^{12}–$10^{13}\,M_{\odot}$) halos at $<1\,R_{\rm vir}$, PATH shows that 5 (1) of them might originate from these halos themselves, but one has DM over 1000 so is unlikely to have a nearby origin. We find seven more FRBs likely associated with the intersected galaxies when focusing on $b < 2\,R_{\rm vir}$, and three FRBs may arise from halos closer to the ones they are found to intersect. We thus performed our measurement of DM excess again without these FRBs identified, and find that our main conclusions remain unchanged. The PATH code, however, is only a rough way of estimating the probability of FRBs being associated with galaxies, and much more careful visual inspection of the locations of galaxies versus the localization contours of FRBs should be done before drawing conclusions.

[12] https://github.com/FRBs/astropath

ORCID iDs

Xiaohan Wu https://orcid.org/0000-0003-2061-4299

References

Aggarwal, K., Budavári, T., Deller, A. T., et al. 2021, ApJ, 911, 95
Amiri, M., Andersen, B. C., Bandura, K., et al. 2021, ApJS, 257, 59
Astropy Collaboration, Robitaille, T. P., Tollerud, E. J., et al. 2013, A&A, 558, A33
Behroozi, P., Wechsler, R. H., Hearin, A. P., & Conroy, C. 2019, MNRAS, 488, 3143
Bhardwaj, M., Gaensler, B. M., Kaspi, V. M., et al. 2021a, ApJL, 910, L18
Bhardwaj, M., Kirichenko, A. Y., Michilli, D., et al. 2021b, ApJL, 919, L24
Boquien, M., Burgarella, D., Roehlly, Y., et al. 2019, A&A, 622, A103
Bregman, J. N., Hodges-Kluck, E., Qu, Z., et al. 2022, ApJ, 928, 14
Burchett, J. N., Elek, O., Tejos, N., et al. 2020, ApJL, 891, L35
Chadayammuri, U., Bogdan, A., Oppenheimer, B., et al. 2022, ApJL, 936, L15
Connor, L., & Ravi, V. 2021, NatAs, 6, 1035
Connor, L., Sievers, J., Pen, U. L., et al. 2016, MNRAS, 458, L19
Cook, A. M., Bhardwaj, M., Gaensler, B. M., et al. 2023, arXiv:2301.03502
Cordes, J. M., & Chatterjee, S. 2019, ARA&A, 57, 417
Cordes, J. M., & Lazio, T. J. W. 2002, arXiv:astro-ph/0207156
Cordes, J. M., Ocker, S. K., & Chatterjee, S. 2022, ApJ, 931, 88
Dai, X., Bregman, J. N., Kochanek, C. S., & Rasia, E. 2010, ApJ, 719, 119
Hallinan, G., Ravi, V., Weinreb, S., et al. 2019, BAAS, 51, 255
Keating, L. C., & Pen, U.-L. 2020, MNRAS, 496, L106
Kirsten, F., Marcote, B., Nimmo, K., et al. 2022, Natur, 602, 585
Kulkarni, S. R., Ofek, E. O., & Neill, J. D. 2015, arXiv:1511.09137
Lee, K.-G., Ata, M., Khrykin, I. S., et al. 2022, ApJ, 928, 9
Lin, H.-H., Lin, K.-y., Li, C.-T., et al. 2022, PASP, 134, 094106
Macquart, J.-P., Prochaska, J. X., McQuinn, M., et al. 2020, Natur, 581, 391
McGaugh, S. S., Schombert, J. M., de Blok, W. J. G., & Zagursky, M. J. 2010, ApJL, 708, L14
McQuinn, M. 2014, ApJL, 780, L33
McQuinn, M. 2016, ARA&A, 54, 313
Moster, B. P., Somerville, R. S., Maulbetsch, C., et al. 2010, ApJ, 710, 903
Naab, T., & Ostriker, J. P. 2017, ARA&A, 55, 59
NASA/IPAC Extragalactic Database (NED) 2019, NASA/IPAC Extragalactic Database (NED)
Nimmo, K., Hessels, J. W. T., Snelders, M. P., et al. 2023, MNRAS, 520, 2281
Niu, C.-H., Aggarwal, K., Li, D., et al. 2022, Natur, 606, 873
Petroff, E., Hessels, J. W. T., & Lorimer, D. R. 2019, A&ARv, 27, 4
Petroff, E., Hessels, J. W. T., & Lorimer, D. R. 2022, A&ARv, 30, 2
Platts, E., Prochaska, J. X., & Law, C. J. 2020, ApJL, 895, L49
Prochaska, J. X., Macquart, J.-P., McQuinn, M., et al. 2019, Sci, 366, 231
Prochaska, J. X., & Zheng, Y. 2019, MNRAS, 485, 648
Ravi, V. 2019, ApJ, 872, 88
Ravi, V., Catha, M., Chen, G., et al. 2023, arXiv:2301.01000
Schaan, E., Ferraro, S., Amodeo, S., et al. 2021, PhRvD, 103, 063513
Tendulkar, S. P., Bassa, C. G., Cordes, J. M., et al. 2017, ApJL, 834, L7
Tumlinson, J., Peeples, M. S., & Werk, J. K. 2017, ARA&A, 55, 389
Vanderlinde, K., Liu, A., Gaensler, B., et al. 2019, Canadian Long Range Plan for Astronomy and Astrophysics White Papers, 2020, 28
Vedantham, H. K., & Phinney, E. S. 2019, MNRAS, 483, 971
White, D. J., Daw, E. J., & Dhillon, V. S. 2011, CQGra, 28, 085016
Williams, I., Khan, A., & McQuinn, M. 2023, MNRAS, 520, 3626
Yang, Y.-P., Luo, R., Li, Z., & Zhang, B. 2017, ApJL, 839, L25
Yao, J. M., Manchester, R. N., & Wang, N. 2017, ApJ, 835, 29